Ionization of a P-doped Si(111) nanofilm using two-dimensional periodic boundary conditions

Tzu-Liang Chan, Alex J. Lee, and James R. Chelikowsky

Phys. Rev. B **91**, 235445 — Published 25 June 2015

DOI: 10.1103/PhysRevB.91.235445

Ionization of a P-doped Si(111) nanofilm using 2D periodic boundary conditions

Tzu-Liang Chan,[1,2,*] Alex J. Lee,[1,3] and James R. Chelikowsky[1,4,3,†]

[1]*Center for Computational Materials,*
Institute for Computational Engineering and Sciences,
University of Texas, Austin, Texas 78712, USA

[2]*Department of Physics, Hong Kong Baptist University,*
Kowloon Tong, Kowloon, Hong Kong

[3]*Department of Chemical Engineering,*
University of Texas, Austin, Texas 78712, USA

[4]*Departments of Physics, University of Texas, Austin, Texas 78712, USA*

Abstract

We examine the ionization of a P dopant in a Si(111) nanofilm using first-principles electronic structure calculations with 2D periodic boundary conditions. The electrostatic divergence of a charged periodic system is resolved by defining an electrostatic reference potential along the confined direction. After ionization, there is an overall electrostatic potential drop of the system. A nanofilm with larger periodicity can reduce the potential drop by screening the P ion, and leads to a smaller ionization energy. We compare the ionization energy calculated for the P-doped Si nanofilm with a P-doped Si nanocrystal and a P-doped Si(110) nanowire. As dimensionality decreases, quantum confinement tends to lower the ionization energy by raising the defect level. However, lower dimensionality also reduces screening after P ionization. This leads to a larger electrostatic potential drop and offsets the effect of quantum confinement on the ionization energy.

PACS numbers: 73.21.Fg, 73.90.+f, 71.15.Dx

I. INTRODUCTION

Electronic components are miniaturizing to the nanoscale in order to pack more functionalities and enhance the speed of electronic devices[1]. The size of a transistor in a CPU is currently in the range of 10-30 nm[2]. It is expected that strong quantum effect will start to dominate the device properties when the semiconductor manufacturing process adopts sub-10 nm technology. There are electrically charged components, for example, bits in the computer memory are determined by whether the capacitors in the DRAM are charged or discharged. A gate capacitor can be used to control the current flow through the channel region of a field effect transistor. Charged nanostructures can also be utilized in miniaturized batteries as a high-power energy storage device due to the fast kinetics of electrons within nanostructures[3] and excellent recyclability.

The electronic properties of a charged nanostructure can be quite different from a macroscopic one. It is known that screening is weaker in a nanomaterial, hence its dielectric constant is typically smaller[4]. A nanocapacitor has a much smaller density of states at the Fermi level. Therefore, charging a nanocapacitor can easily affect its Fermi level, thus its capacitance varies with its charge state[5]. Moreover, it is expected that its charging behavior can be strongly affected by its detailed atomic structure and the interface structure of the surrounding material. Unfortunately, the electronic properties of charged nanostructures have yet to be fully explored even theoretically. This is because charged nanostructures pose technical difficulties to first-principles electronic structure calculations. Nanowires and nanofilms are typically modelled as periodically repeating structures. A charged periodic structure has a divergent electrostatic energy[6]. The divergence originates from the long-range Coulomb interaction, which becomes divergent when all the contributions from the periodic images are added up. The issue can also be interpreted as the problem of defining an electrostatic reference potential. Conventionally, the reference is defined to be zero infinitely far away. If the system is charged but also infinite in extent, it becomes problematic to define the reference at a location where charges are located.

The divergent electrostatic energy of a charged nanowire or nanofilm is actually an artifact and does not exist in experiments because all charged nanostructures have a finite size. The periodicity is imposed for convenience theoretically. A typical approach to resolve the issue is to remove the divergence and correct the total energy to recover a value that is physically

meaningful. Popular first-principles electronic structure codes use plane waves as a basis set, which imposes three-dimensional periodicity to the system. Plane wave codes set the average electrostatic potential of the system to be zero. This corresponds to introducing a jellium background into the unit cell to neutralize the charged system[7]. The total energy can be corrected by the Madelung sum[8,9], which evaluates the electrostatic interaction between the periodic net charges of the system and the inserted jellium. Long-range Coulomb interactions due to dipoles, quadrupoles and higher-order multipoles within a unit cell can be corrected by the Makov and Payne scheme[10] or compensated by introducing Gaussian charges[11] and local moments[12,13] into the system.

If the absolute value of the total energy is not important, for example when comparing total energies, then it is only necessary to calculate the total energies with respect to the same electrostatic reference potential. This motivates the potential alignment technique: the electrostatic potential of a small region of the unit cell can be aligned to a chosen value[14–16]. The alignment procedure is equivalent to choosing a common reference vacuum energy level. Total energy correction schemes can be coupled with potential alignment[17]. Using ZnO and GaAs as prototypical systems, Zunger *et al.* demonstrated that the Makov-Payne correction accompanied by a potential alignment scheme can lead to well-converged formation energies of charged defects[18].

There are computational schemes designed specifically for charged nanostructures with three-dimensional periodicity imposed. The total energy of a charged nanowire can be corrected by a generalized Madelung correction[19]. However, it is found that the total energies converge quite slowly with unit cell size[20]. Unless the intention is to simulate an array of nanowires, the imposed periodicity perpendicular to the wire axis is superfluous. There are efforts trying to eliminate the effect of this extra periodicity (while still using plane wave codes) by the Coulomb-cutoff method[21–24], which truncates the long-ranged Coulomb interaction or restricting the wave functions along the directions perpendicular to the nanowire[25–27]. The interactions along the perpendicular directions can also be corrected by a corrective potential[28]. There are similar approaches for charged nanofilms. For example, charged films can be neutralized by jellium or countercharge sheets[29]. The inter-film dipole interactions can be evaluated and eliminated[30–32].

In this paper, we shall develop a computational algorithm specifically designed for charged two-dimensional periodic nanofilms. Our algorithm is based on PARSEC[33,34], which is a first-

principles electronic structure code using a real-space grid instead of a plane wave basis set. PARSEC has already been implemented a partially periodic boundary condition such that the system is only periodic along the x and y directions, but confined along the z direction[35]. The advantage of such a computational approach is that the inter-film interaction does not even exist, therefore it is not necessary to devise schemes trying to eliminate such interactions. Another advantage is the flexibility on imposing boundary conditions along the z direction. Since the z direction is not periodic, we are free to impose any physical boundary conditions on the top and the bottom surfaces of the unit cell to simulate various experimental conditions. Our new contribution is to make use of this flexibility to address the issue of charged nanofilms. We shall use the boundary condition to define an electrostatic reference potential. The reference can be defined consistently for different calculations such that different total energies are comparable and the electronic structures are aligned. A similar approach has been adopted for a charged nanowire calculated using a one-dimensional periodic boundary condition[36].

As a case study, we examined an ionized SiH_4 molecule. The boundary condition is designed such that the total energy and the electronic structure of the ionized molecule is the same as those using a non-periodic confined simulation cell. We then illustrate our scheme to study the ionization of a P-doped Si(111) nanofilm. After the P dopant is ionized, there is an overall electrostatic potential drop of the system. The Si nanofilm can reduce the potential drop by screening the P ion. As the nanofilm periodicity increases, we find that the potential drop becomes smaller and the ionization energy lowers accordingly. The dependence on periodicity can also be seen with a classical simulation of a positive charge embedded in a dielectric slab. Finally, we compare the ionization energy of the P dopant in the nanofilm with that in a nanowire or a nanocrystal. As the dimensionality decreases, quantum confinement tends to lower the ionization energy by raising the defect level, but it is not sufficient to offset the increase of the ionization energy owing to reduced screening.

II. THE 2D PERIODIC KOHN-SHAM PROBLEM WITH A NET CHARGE

The treatment of a neutral system with 2D periodic boundary conditions was described in detail in Ref. 35. In this section, a brief review of the formalism will be given together with our new modification to handle a charged system. Consider a two-dimensional periodic

system with periodicity L_x and L_y along the x and y directions, respectively. Its electronic structure can be obtained by solving the Kohn-Sham equation[37,38]:

$$\left(\frac{-\hbar^2\nabla^2}{2m} + V_{ion}(\mathbf{r}) + V_H[\rho] + V_{xc}[\rho]\right)\psi_{n,k_x,k_y}(\mathbf{r}) = \varepsilon_{n,k_x,k_y}\psi_{n,k_x,k_y}(\mathbf{r}). \tag{1}$$

V_{ion} is the ion-core pseudopotential, and we adopt the Troullier-Martins pseudopotentials[39] in the Kleinman-Bylander form[40]. V_H is the Hartree potential, which is obtained by solving the Poisson equation for a given electronic charge density ρ. V_{xc} is the exchange-correlation potential. In this study, the local density approximation (LDA) is used, and V_{xc} adopts the Ceperley and Alder functional[41] parameterized by Perdew and Zunger[42]. The system of interest is enclosed by a rectangular box periodic along both the x and y directions, but the z direction is confined. The height L_z of the box should be large enough to contain the system plus a sufficient amount of vacuum space (at least 3-4 Å) such that the wave functions ψ_{n,k_x,k_y} decay to 0 at the top and bottom of the box. For a 2D periodic system, the solutions are labeled by the band index n and a wave vector (k_x, k_y) in the first Brillouin zone by the Bloch theorem[43]. In this paper, we focus on isolated charged dopants such that the lateral dimension of the box L_x and L_y are large and only the Γ point is used to sample the Brillouin zone. Our algorithm for studying charged periodic systems applies to any two-dimensional periodic systems in general. The Kohn-Sham equation should be solved self-consistently since V_H and V_{xc} depend on the unknown ρ.

The central issue of a charged periodic system is that its electrostatic energy diverges. Hence, we focus on how the electrostatic potential is dealt with in the Kohn-Sham equation. $V_{ion} + V_H$ comprise the electrostatic part of the self-consistent potential V_{SCF}. The idea is to add and subtract a compensating potential V_{com} to the electrostatic potential as $(V_{ion} + V_{com}) + (V_H - V_{com})$. V_{com} neutralizes V_{ion} such that the electrons in the system are under the influence of an electrically neutral ionic potential $(V_{ion} + V_{com})$. The electrostatic divergence is handled when we solve the Poisson equation for $(V_H - V_{com})$.

For the nth atom with ionic charge Z_n in the system, we overlay at the atomic position a potential of the form

$$v^n_{com} = \frac{-Z_n}{r}\,\mathrm{erf}\left(\frac{r}{\sqrt{2}\sigma_n}\right). \tag{2}$$

r is the radial distance from the atom. The potential corresponds to the electrostatic potential of a Gaussian charge with width σ_n. σ_n is chosen to be half of the cutoff radius of the atom's pseudopotential. This way, the added potential can roughly cancel the pseudopoten-

tial beyond the cutoff radius. V_{com} is to sum v_{com}^n over all the atoms within the unit cell. Since the Gaussian charge is opposite to the ionic charge, $(V_{ion} + V_{com})$ corresponds to the potential of a neutral system. Therefore, its influence to an electron will not be long-ranged. $(V_{ion} + V_{com})$ within the unit cell can be evaluated by summing over the periodic images of the system. The choice of σ_n affects how many periodic images are needed in the sum. For our choice above, only a few periodic images is sufficient to converge the sum.

The Hartree potential can be solved by the Poisson equation

$$\nabla^2 V = -4\pi \left(\rho - \rho_{com}\right) = -4\pi\rho^{tot}. \tag{3}$$

ρ_{com} is the sum of all the Gaussian charges added when we evaluate $(V_{ion} + V_{com})$ above. Thus, the solution of the Poisson equation V corresponds to $(V_H - V_{com})$. V_{com} will be cancelled out in the Kohn-Sham equation without any physical effect. The boundary condition for the Poisson equation is specified as follows. For each plane z_i within the unit cell, a Fourier transform is performed for the planar charge density $\rho^{tot}(z_i)$. For a point $\vec{r} = (x, y, z)$ at the top or the bottom of the calculation domain, the Fourier component $\rho_{0,0}^{tot}$ contributes $-2\pi\rho_{0,0}^{tot}|z - z_i|$ to $V(\vec{r})$. The other Fourier components $\rho_{l,m}^{tot}$ contribute $2\pi\frac{\rho_{l,m}^{tot}}{|\vec{k}_{l,m}|}e^{i\vec{k}_{l,m}\cdot\vec{r}}e^{-|\vec{k}_{l,m}||z-z_i|}$ to $V(\vec{r})$[44]. Here, $\vec{k}_{l,m} = (l\frac{2\pi}{L_x}, m\frac{2\pi}{L_y}, 0)$, where l and m are integers. The contribution of ρ^{tot} from all the planes z_i should be summed up to obtain $V(\vec{r})$ at the boundary. For example, if ρ^{tot} is a uniformly charged plate at $z_i = 0$, then the boundary condition is simply $-2\pi\rho_{0,0}^{tot}|z|$. The electrostatic potential varies linearly with z and diverges infinitely far away. We can see that the reference potential is set to be the location of the charged plate. Such treatment of two-dimensional periodic systems was adopted in Ref. 35. For a neutral system, it is known that the definition of the reference potential is not crucial because it will be cancelled out in the total energy[45]. However, if the system is charged, the total energy will depend on how the reference is defined. In fact, the above specification of the boundary condition for the Poisson equation is equivalent to setting the self-interaction energy of a two-dimensional array of charges to be zero. In this paper, we propose to take into account the self-interaction energy contribution to the boundary condition of the Poisson equation. Later, we shall show that the eigenvalue spectrum and the total energy of a charged molecule inside a two-dimensional periodic cell will be the same as an isolated charged molecule.

Suppose a system has a net charge $Z_{net} = Z_{ion} - Z_e$, where Z_{ion} is the total ionic charge

and Z_e is the total number of electrons. In addition to the boundary condition of the Poisson equation specified above, we can shift the electrostatic potential at the boundary by an amount $2Z_{net}E_{self}$. E_{self} is the self-interaction energy of a charge placed in a two-dimensional rectangular box with periodicities L_x and L_y (with the divergence removed)[46]:

$$E_{self} = \left(8 \sum_{i,j} K_0 \left(2\pi ij \frac{L_y}{L_x} \right) - 2 \log \left(4\pi \frac{L_x}{L_y} \right) + 2\gamma \right) / L_x. \tag{4}$$

K_0 is the modified Bessel function of the second kind. γ is the Euler constant 0.5772. The shift depends on the size of the box and redefines the reference for the electrostatic potential. As a result, V_{SCF} of the Kohn-Sham equation and the eigenvalue spectrum will be shifted by the same amount. The total energy E_{total} is given by:

$$E_{total} = \sum_{\mathbf{k}} \sum_{n=1}^{occ(\mathbf{k})} \varepsilon_{n,\mathbf{k}} - \frac{1}{2} E_H + \int \rho(\mathbf{r}) \left(\varepsilon_{xc} \left[\rho(\mathbf{r}) \right] - V_{xc} \left[\rho(\mathbf{r}) \right] \right) d^3\mathbf{r} + E_{ion}. \tag{5}$$

The band energy is to sum over all the occupied eigenvalues $\varepsilon_{n,\mathbf{k}}$, and is shifted by an amount $2Z_{net}Z_eE_{self}$. $E_H = \int V_H(\mathbf{r}) \rho(\mathbf{r}) d^3\mathbf{r}$ is the Hartree energy. E_H describes the energy of the electronic charge density $\rho(\mathbf{r})$ under the electrostatic potential $V_H(\mathbf{r})$ due to the electrons themselves. Both ρ and V_H do not include the contribution from the Gaussian compensation charges. After taking into account the self-interaction of the electrons between the periodic cells, V_H is shifted by $-2Z_eE_{self}$ with E_H adjusted accordingly by an amount $-2Z_e^2E_{self}$. The negative sign is because the adjustment of the electrostatic boundary condition is opposite for ion-electron and electron-electron interactions. ε_{xc} is the exchange-correlation energy density which is unaffected by the electrostatic boundary condition. Finally, the change to the ion-ion Coulomb interaction energy E_{ion} is $-Z_{ion}^2E_{self}$. If the system is electrically neutral ($Z_{ion} = Z_e$), both the eigenvalue spectrum and the total energy will be unchanged as expected. It is straight forward to show that the net adjustment to the total energy is $-Z_{net}^2E_{self}$ when the system carries a net charge. There is no change to the force evaluation because only a constant shift to E_{total} is introduced.

III. IONIZATION OF A SiH_4 MOLECULE

To demonstrate how the scheme works, we calculated an ionized SiH_4 (silane) molecule in a two-dimensional periodic box. An electron is removed from the molecule such that

$Z_{net} = 1$. The molecular structure is kept fixed in this study. Since the goal here is not to study the detailed chemistry of SiH_4, but how the eigenvalue spectrum and the total energy change with the box size, we performed non-spin polarized calculations for simplicity.

For the SiH_4^+ molecule in a periodic box with $L_x = L_y = 20$ a.u., Fig. 1(a) depicts the variation of V_{SCF} from the position of the molecule to the top of the box. At a height sufficiently far away from the SiH_4^+, the periodically repeating charged molecule starts to resemble a uniformly charged plane, and V_{SCF} increases linearly with height. The electrostatic potential of a uniformly charged plane $\frac{4\pi}{L_x L_y} z$ is plotted as a comparison. The line is shifted by $2Z_{net}E_{self}$ such that both curves correspond to the same electrostatic reference. The total energy of SiH_4^+ is plotted as a function of box size in Fig. 1(b). Along the confined z direction of the box, E_{tot} converges quickly with a few Å of vacuum space between the molecule and the edge of the box. Along the periodic x and y directions, the wave functions between adjacent periodic cells can overlap, but separating the periodic molecules with ∼10 Å of vacuum space is sufficient to converge E_{tot}. The converged value of E_{tot} corresponds nearly exactly to the result of a SiH_4^+ molecule in a non-periodic confined box. The quick convergence is made possible by shifting the electrostatic reference using the self-interaction energy as detailed in the previous section. Without the shift, the convergence of E_{tot} with L_x and L_y will be very slow.

In our scheme, not only E_{tot} is corrected, but the eigenvalue spectrum is properly aligned at the same time. In Fig. 1(c), we plot the spectrum for different periodicities $L_x = L_y = L$. Only the lowest eight eigenvalues are presented. Apparently, only four eigenvalues can be observed because ε_2 to ε_4 are degenerate, so are ε_5 to ε_7. The $L = \infty$ case corresponds to the spectrum of a SiH_4^+ molecule in a non-periodic confined box. We can see that all the eigenvalue spectrums are respect to the same electrostatic reference such that they can be compared directly. The convergence is similar to that in Fig. 1(b). The convergence for the unoccupied states (ε_5 to ε_8) is slightly slower because they split as the more extended wave functions overlap between the periodic images.

IV. IONIZATION OF A P-DOPED Si(111) NANOFILM

We apply our scheme to an ionized P dopant embedded in a Si(111) nanofilm. As illustrated in Fig. 2, our Si(111) slab consists of 6 Si atomic layers. Each surface Si atom has

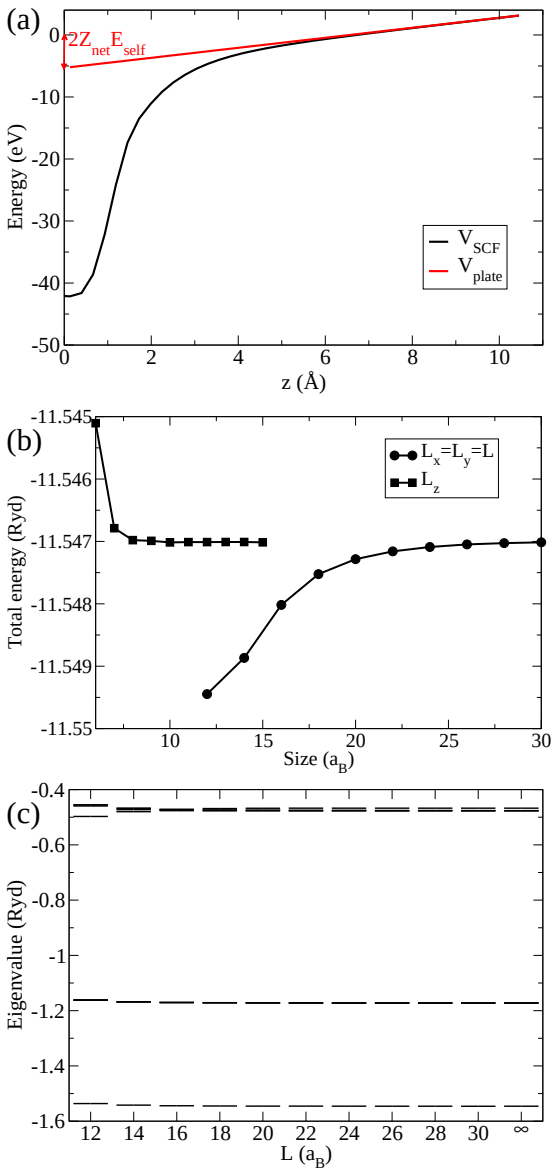

FIG. 1. (a) The self-consistent potential V_{SCF} plotted from the SiH_4^+ position ($z = 0$) to the top of the simulation box. The variation of V_{SCF} approaches the electrostatic potential of a uniformly charged sheet V_{plate} for sufficiently large z. $V_{plate} = 4\pi\sigma z + 2Z_{net}E_{self}$, where $\sigma = \frac{1}{L_x L_y}$ is the surface charge density, $Z_{net} = 1$ and E_{self} is defined in Eqn. 4. The second term in V_{plate} corresponds to our choice of the electrostatic reference potential. (b) The total energy E_{tot} of SiH_4^+ plotted as a function of the height of the simulation cell L_z (■, $L_x = L_y$ fixed at 30 a_B) and the periodicity $L_x = L_y = L$ (•, L_z fixed at 15 a_B). (c) The variation of the eigenvalue spectrum of SiH_4^+ with the periodicity L. The spectrum for $L = \infty$ corresponds to the result from a non-periodic confined calculation.

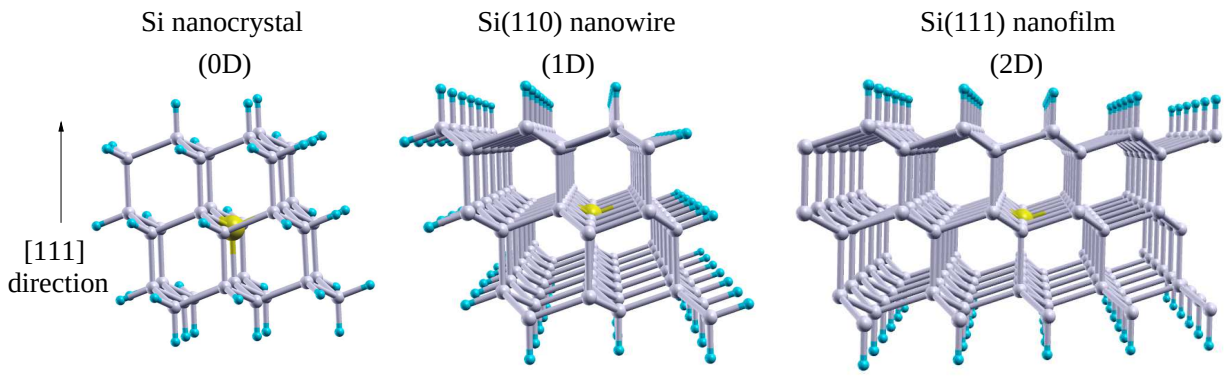

FIG. 2. The atomic geometry of a P-doped Si nanocrystal, Si(110) nanowire and Si(111) nanofilm. The three structures are oriented such that the (111) direction is pointing upwards, and the (110) direction is into the paper. The Si atoms are colored grey, and the cyan atoms are the H passivation. The large yellow atoms at the center of the structures are the P substitutional dopants.

only one dangling bond, which is passivated by a H atom. One of the Si atoms close to the center of the slab is substituted by a P atom. The P atoms are covered by 2-3 layers of Si and the P are well separated from each other such that the effect of P is to introduce a defect level into the Si band gap. The P-doped Si nanofilm is ionized by removing an electron from the defect level, which is the highest occupied energy level of the system. Although the film thickness is small, our purpose here is not to simulate a Si surface, but to illustrate our scheme for the case of a charged nanofilm. In our study, the Si atoms are kept fixed at their bulk positions without atomic relaxation. Here, we want to study the ionization energy of the P dopant in the Si(111) nanofilm. Previous studies on a similar system show that atomic relaxation has a minor effect on the ionization of the P atom[47]. In general, spin-polarized calculations are required for defect states. Here, we only performed non-spin-polarized calculations as in the SiH_4^+ study. This is because the ionization energies differ by at most 0.01 eV even if spin polarization is included at the LDA level.

For our test case using SiH_4^+ molecule, our adjustment of the electrostatic reference recovers the eigenvalue spectrum and the total energy of an isolated non-periodic molecule. The Coulomb interaction among the charged molecules are removed by the reference. An analogous interpretation for the ionized P-doped Si nanofilm is that the total energy corresponds

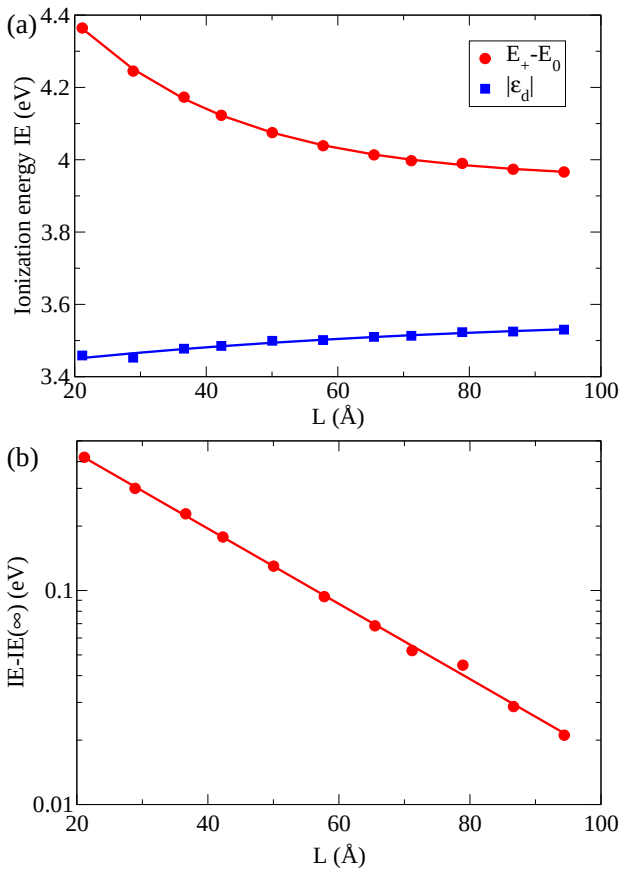

FIG. 3. (a) The ionization energy IE of the P-doped Si(111) nanofilm as a function of the periodicity L. The • curve uses a total energy approach. The eigenvalue of the defect level $|\varepsilon_d|$ when the system is neutral (■) is plotted for comparison. (b) IE exhibits an exponential decay with L. This is verified by a linear dependence when the • curve is plotted on a log-linear scale.

to a periodic film but with the Coulomb interaction among the P ions removed. Physically, this can be related to a finite Si(111) slab of size $L_x \times L_y$. Note that this association is not exact because our periodic model is continuous without the four edges around a finite slab. However, the total energy of our periodic model does progressively approach a finite one when L_x and L_y are getting larger.

For a P-doped Si(111) nanofilm with periodicity $L_x \approx L_y = L$, we calculate its ionization energy IE by

$$IE = E_+ - E_0. \tag{6}$$

E_+ is the total energy of an ionized P-doped Si(111) film. E_0 is the total energy of the same system without the ionization. IE corresponds to the energy required to extract the

defect electron from the doped Si nanofilm to the vacuum. Fig. 3(a) shows the variation of IE with L (the film thickness is fixed). IE increases with decreasing L. A similar trend can also be observed for a P-doped Si(110) nanowire with different axial periodicity[36]. The curve can be fitted very well using an exponential function of the form:

$$IE = IE(\infty) + \Delta \exp(-L/\lambda). \tag{7}$$

In Fig. 3(b), the corresponding log-linear plot indicates a nearly straight line, which shows that its L dependence is indeed exponential. The asymptotic value $IE(\infty)$ for large L is extrapolated to be 3.95 eV. The decay length λ is fitted to be 24.7 Å. Δ represents the effect of L on IE.

In Fig. 3(a), IE is compared with the eigenvalue of the P defect level $|\varepsilon_d|$ when the system is neutral. According to the Janak's theorem[48], $\varepsilon_d = \frac{\partial E_{tot}}{\partial n_d}$. ∂n_d corresponds to a differential change in the occupancy of the defect level. Note that ε_d lowers as n_d reduces from 1 to 0 in LDA. IE should correspond to $\int_1^0 \varepsilon_d\,(n_d)\,dn_d$. In the neutral state, the $|\varepsilon_d|$ in Fig. 3(a) does not take into account the lowering of the defect level as its occupancy changes. IE exhibits a change of ∼0.4 eV for the range of periodicity L examined in Fig. 3, while $|\varepsilon_d|$ shows little variation with L. Therefore, $|\varepsilon_d|$ does not take into account the long-ranged phenomena after P ionization. In the next section, we shall show that a classical electrostatic model of a positive charge embedded in a dielectric can qualitatively reproduce the trend. This implies that the final-state effects such as an electrostatic potential drop and polarization around the P dopant after ionization are not included in $|\varepsilon_d|$. The small variation of $|\varepsilon_d|$ with L is related to the overlap of the defect wave function Ψ between periodic cells. Fig. 4(a) shows that Ψ is quite localized around the P dopant. Ψ along the z direction is significantly confined by the nano thickness of the Si(111) slab (Fig. 4(b)). Fig. 4(c) illustrates the radial dependence of Ψ, which decays roughly exponentially from the P. By integrating along the radial direction, Fig. 4(d) shows that most of the defect charge density is within a 2-3 nm radius from the P dopant. The overlap of Ψ between periodic cells should not be significantly enough to modify IE by ∼0.4 eV in Fig. 3. It is well-known that LDA predicts too small a band gap[49]. In our study, the thickness of the Si film is fixed. As such, the band gap and the confinement of Ψ within the film remains the same as L changes. Therefore, the LDA error should only give rise to a systematic shift of ε_d in Fig. 3(a). While the long-range tail of Ψ is also prone to the self-interaction error of LDA[50], it should not affect our analysis

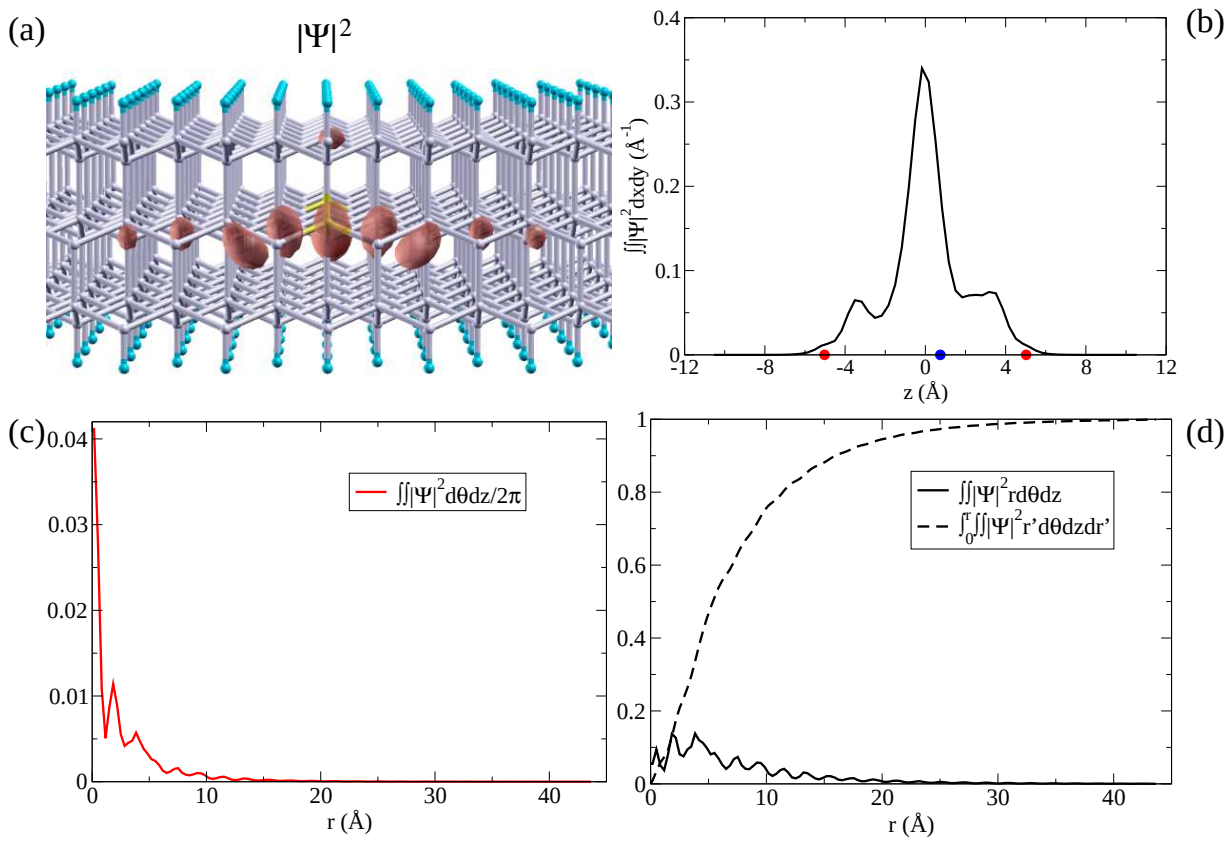

FIG. 4. (a) A contour plot of the P defect wave function $|\Psi|^2$. The red contour corresponds to the value 0.005 Å^{-3}. (b) The variation of $|\Psi|^2$ is plotted against z (after integrating with respect to x and y). The blue dot on the x-axis denotes the P location, and the two red dots correspond to the z coordinates of the H passivation. (c) The average variation of $|\Psi|^2$ against the radial distance r (in cylindrical coordinates with θ and z dependence integrated out). (d) $|\Psi|^2 r$ is plotted against r (solid line). Its integral (dashed line) shows that Ψ is normalized.

qualitatively.

Thus, the large variation of IE with L as observed in Fig. 3(a) is mostly a consequence of final-state effects, *i.e.* how the ionized P dopant is screened by the Si nanofilm. One such final-state effect is the electrostatic potential drop ΔV of the system after the ionization. Fig. 5 depicts the density of states of the P-doped Si(111) nanofilm before and after ionization for two different periodicities L. ΔV can be seen from the overall downward shift of the potential. $\Delta V \approx 1.7$ eV in Fig. 5(a) with a smaller L is larger than $\Delta V \approx 0.5$ eV in Fig. 5(b). A larger ΔV leads to a larger IE for small L in Fig. 3(a). ΔV is related to the

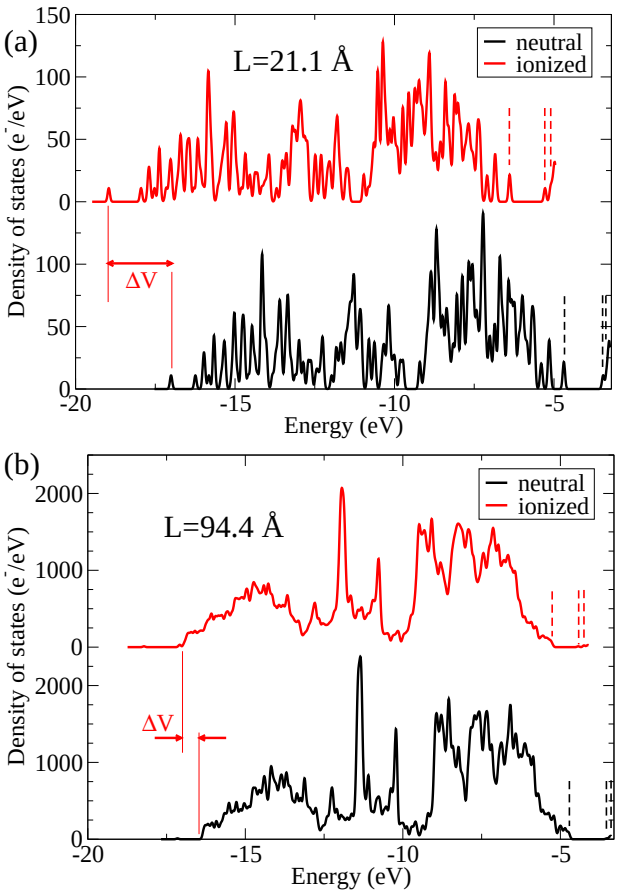

FIG. 5. The density of states of the P-doped Si(111) nanofilm before and after ionization of the P dopant. There is an electrostatic potential drop of the system as a whole after ionization. The drop is larger for a nanofilm with a smaller periodicity (a) $L = 21.1$ Å compared to the nanofilm with (b) $L = 94.4$ Å. The three vertical dashed lines denote (from left to right) the energies of the valence band maximum, the defect level and the conduction band minimum, respectively.

screening of the P ion by the Si nanofilm. A smaller L corresponds to a smaller piece of dielectric to screen the positive charge.

V. A LINEAR DIELECTRIC MODEL OF AN IONIZED Si FILM

To examine the effect of screening, we perform a classical electrostatic simulation of a positive charge embedded in a dielectric slab, and see if the classical simulation can reproduce the observed trend of IE versus L. In our classical model, the positive charge is represented

by a Gaussian charge distribution of the form:

$$\rho_G(r) = \frac{1}{\sqrt{2\pi}\sigma} \exp\left(-\frac{2r^2}{\sigma^2}\right) \tag{8}$$

σ is chosen to be 2 a_B, which corresponds roughly to the size of an atom. ρ_G is centered at the origin and embedded inside a dielectric slab with dielectric constant K. The slab has a thickness t with periodicity L along both the x and y directions. The dielectric constant κ of the space does not drop abruptly from K to the vacuum value 1 across the interface. Instead, it changes smoothly along the z direction with a smearing δ at the interface $z = \frac{t}{2}$:

$$\kappa(z) = \frac{K-1}{\exp\left(\frac{z-\frac{t}{2}}{\delta}\right)+1} + 1 \tag{9}$$

for $z > 0$. κ is defined similarly for $z < 0$. δ is chosen to be 0.5 a_B. Here, δ is mostly for numerical convenience. Physically, the Si-vacuum interface is also not abrupt with a H passivation in between. κ has no x and y dependence. The generalized Poisson equation[51]

$$\nabla \cdot (\kappa \nabla V) = -4\pi\rho_G \tag{10}$$

is solved because the dielectric constant varies in space. The boundary condition for the Poisson equation is set in the same way as our first-principles electronic structure calculations and the electrostatic reference potential is set using E_{self} in Eqn. 4 as well.

After the Poisson equation is solved, the electrostatic potential at the origin $V(0,0,0)$ is extracted. We calculate the ionization energy IE by $\frac{1}{2}QV(0,0,0)$. Here, $Q = 1$ in atomic units. The formula approximates the energy needed to create ρ_G within the dielectric slab. Our plan is to study how IE varies with the periodicity L classically, and compare with our first-principles result. Our classical model has two parameters: t and K. The slab thickness t can be chosen roughly equal to the thickness of the H-passivated Si(111) slab. Note that the thickness is not really well defined in the nanoscale. For K, it is known that the dielectric constants of nanostructures are usually smaller than the bulk value[4]. Here, we determine t and K such that the L dependence of IE is similar between the first-principles and classical simulations. By fitting our classical results by Eqn. 7, we try to find t and K such that the classical IE has a similar Δ and λ as our first-principles results.

First, we find that the classical IE does have an exponential L dependence (see Fig. 6(a)). This verifies that the L dependence of IE is related to screening in the Si nanofilm. In Fig. 6(b), we illustrate how Δ and λ change with the parameters t and K in our classical

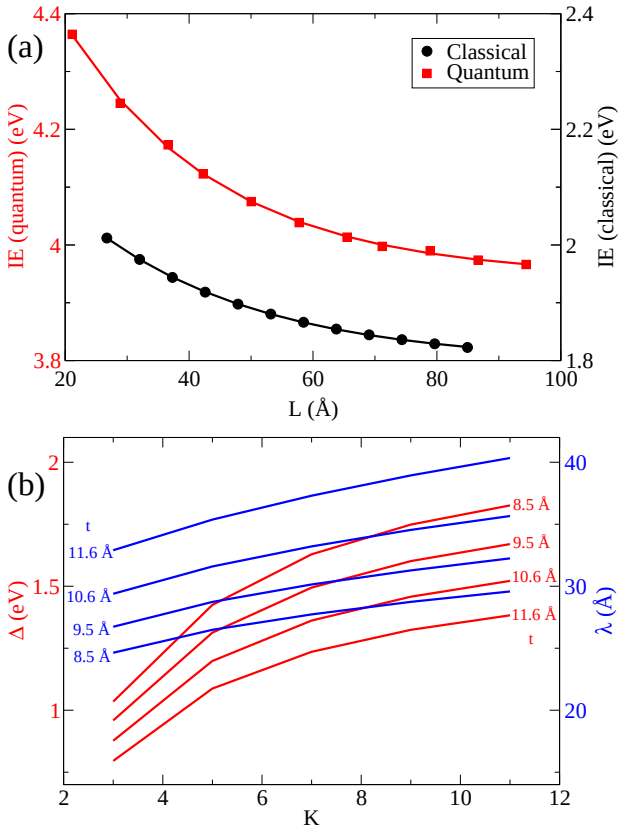

FIG. 6. (a) The ionization energy IE versus nanofilm periodicity L. IE is calculated from either first-principles (quantum) or classical simulations. (b) The IE(classical) results can be fitted to an exponential function of the form $IE\,(\infty) + (\Delta)\exp(-L/\lambda)$. Δ (red curves) and λ (blue curve) depend on the thickness t and the dielectric constant K of the dielectric slab used in the classical simulations. K is along the x-axis. The numbers within the plot are different values of t. The classical curve plotted in (a) corresponds to $t = 9.7$ Å and $K = 3.8$.

simulations. Qualitatively, λ increases with dielectric constant K and film thickness t, while Δ increases with larger K but smaller t. We found it impossible to fit K and t exactly to Δ and λ from first-principles. A close fit can be obtained by choosing $K = 3.8$ and $t = 9.7$ Å. This t corresponds well to the geometry of the Si nanofilm, and the K is smaller than the bulk value of 11.4 as expected. IE as a function of L is plotted in Fig. 6(a) for both first-principles (quantum) and classical simulations. With a suitable choice of K and L, the trend of both curves can be made quite similar to each other. We can notice that the classical value of IE is ∼2 eV lower than the first-principles IE. This is expected because the classical model does not contain information regarding the electronic structure of P-

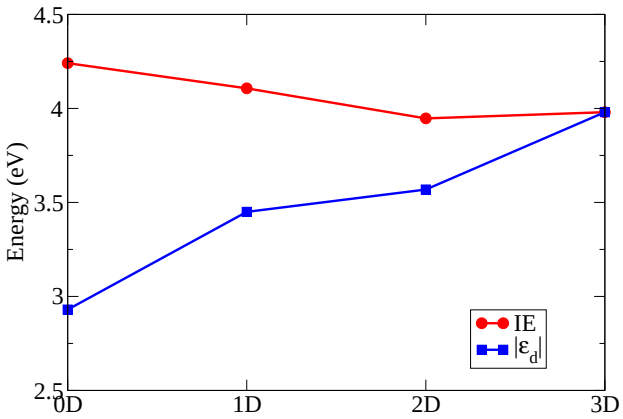

FIG. 7. Comparison of the ionization energy IE (•) between different P-doped Si structures: a Si nanocrystal (0D), a Si(110) nanowire (1D), a Si(111) nanofilm (2D), and a Si bulk crystal (3D). The P-doped nanostructures are illustrated in Fig. 2. The defect levels $|\varepsilon_d|$ of the P-doped Si structures (■) are plotted as well.

doped Si. Moreover, ρ_G as a model of a P atom in Si is probably too crude to reproduce the correct IE value.

VI. COMPARISON BETWEEN P-DOPED Si NANOSTRUCTURES

The role of quantum confinement in dopant ionization can be assessed by comparing the ionization energy IE of a P-doped Si(111) nanofilm with other P-doped Si nanostructures. A P-doped Si nanocrystal and a P-doped Si(110) nanowire are illustrated in Fig. 2. All three nanostructures are constructed such that there are six Si atomic layers in the (111) direction. The Si(111) nanofilm is a two-dimensional periodic structure. The nanowire can be carved out from the nanofilm such that it is one-dimensional periodic along the (110) direction. The Si nanocrystal is roughly a spherical fragment of the nanowire. All three nanostructures have their dangling bonds passivated by H atoms. One of the Si atoms at the center of each nanostructure is substituted by a P atom.

IE is calculated by Eqn. 6 for all the P-doped structures. For the nanowire and nanofilm, the IE corresponds to the asymptotic values as the periodicity $L \to \infty$. The nanocrystal was examined using a confined non-periodic boundary condition. The results for the bulk three-dimensional periodic Si crystal corresponds to that of a P-doped Si nanocrystal with

its radius extrapolated to infinity. IE as a function of dimensionality in plotted in Fig. 7. 0D, 1D, 2D and 3D correspond to the nanocrystal, nanowire, nanofilm and bulk crystal, respectively. The 2D case is examined in this paper. The other cases were examined in our previous studies[36,47,52]. Note that the value for 3D bulk is provided as a reference. Its value can depend on the construction and the surfaces of the nanocrystals used to extrapolate to the bulk crystal.

The trend of the defect level $|\varepsilon_d|$ is plotted as well for comparison. $|\varepsilon_d|$ decreases from 3D bulk to 0D nanocrystal, which is a consequence of quantum confinement on the defect level. The 3D bulk value is also an extrapolation using P-doped Si nanocrystals. The final state effects after the dopant ionization corresponds to the difference between the $|\varepsilon_d|$ and IE curves. Contrary to $|\varepsilon_d|$, the IE curve exhibits an opposite trend with dimensionality. As the bulk crystal is truncated to a nanocrystal, there is a corresponding larger drop in the electrostatic potential ΔV owing to reduced screening. The reduced screening offsets the effect of quantum confinement on $|\varepsilon_d|$. As the influence of screening is found to be slightly stronger, there is a mild rise of IE from 3D bulk to 0D nanocrystal ($\sim$0.25 eV).

VII. CONCLUSION

We examined the ionization of a P-doped Si(111) nanofilm with periodicity L. Since the electrostatic reference for a charged periodic system is divergent and thus not well-defined, we devised a boundary condition for studying the charged nanofilm. The boundary condition sets the electrostatic reference potential which takes into account the electrostatic self-interaction of a two-dimensional periodic array of charges. We found that the total energy of an ionized nanofilm effectively corresponds to a film with finite size L. A larger L can screen the P ion better and lower the ionization energy. This picture is confirmed by a comparison with classical electrostatics simulations using a positive Gaussian charge in a dielectric slab. Finally, we compared the ionization energy IE of various P-doped Si nanostructures constructed in a similar manner. We found that IE increases slightly as more directions are becoming confined. This is a consequence of quantum confinement on the defect level, which lowers IE, and reduced screening leading to a larger electrostatic potential drop that raises IE.

ACKNOWLEDGMENTS

The authors would like to express their appreciation to Jiaxin Han for many useful inputs and valuable discussions. AJL and JRC would like to acknowledge partial support from the U.S. Department of Energy (DoE) for work on nanostructures from grant DE-FG02-06ER46286, and support provided by the Scientific Discovery through Advanced Computing (SciDAC) program funded by U.S. DoE, Office of Science, Advanced Scientific Computing Research and Basic Energy Sciences under award number DE-SC0008877 on algorithms. Computational resources are provided in part by the National Energy Research Scientific Computing Center (NERSC) and the Texas Advanced Computing Center (TACC). TLC acknowledges financial support from Hong Kong Baptist University under grant FRG2/13-14/034, and computational resources provided by the High Performance Cluster Computing Center (HPCCC) at Hong Kong Baptist University, which receives funding from the Research Grant Council, University Grant Committee of the HKSAR and the Hong Kong Baptist University.

---

* tlachan@hkbu.edu.hk

† jrc@utexas.edu

[1] W. Lu, and C. M. Lieber, Nature Mater. **6**, 841 (2007).

[2] I. Ferain, C. A. Colinge, and J.-P. Colinge, Nature **479**, 310-316 (2011).

[3] T.-L. Chan, and J. R. Chelikowsky, Nano Lett. **10**, 821-825 (2010).

[4] D. R. Penn, Phys. Rev. **128**, 2093 (1962).

[5] T.-L. Chan, Phys. Rev. B **86**, 245414 (2012).

[6] W. R. L. Lambrecht, Physica status solidi b **248**, 1547-1558 (2011).

[7] M. Leslie, and N. J. Gillan, J. Phys. C **18**, 973 (1985).

[8] A. F. Wright, and N. A. Modine, Phys. Rev. B **74**, 235209 (2006).

[9] C. W. M. Castleton, A. Hoglund, and S. Mirbt, Phys. Rev. B **73**, 035215 (2006).

[10] G. Makov, and M. C. Payne, Phys. Rev B **51**, 4014-4022 (1995).

[11] P. E. Blochl, J. Chem. Phys. **103**, 7422 (1995).

[12] P. A. Schultz, Phys. Rev. B **60**, 1551-1554 (1999).

[13] P. A. Schultz, Phys. Rev. Lett. **84**, 1942-1945 (2000).

[14] C. Persson, Y.-J. Zhao, S. Lany, and A. Zunger, Phys. Rev. B **72**, 035211 (2005).

[15] D. B. Laks, C. G. Van de Walle, G. F. Neumark, P. E. Blochl, and S. T. Pantelides, Phys. Rev. B **45**, 10965-10978 (1992).

[16] T. Mattila, and A. Zunger, Phys. Rev. B **58**, 1367-1373 (1998).

[17] C. Freysoldt, J. Neugebauer, and C. G. Van de Walle, Phys. Rev. Lett. **102**, 016402 (2009).

[18] S. Lany, and A. Zunger, Phys. Rev. B **78**, 235104 (2008).

[19] R. Rurali, and X. Cartoixa, Nano Lett. **9** 975, 2009.

[20] R. Rurali, M. Palummo, and X. Cartoixa, Phys. Rev. B **81**, 235304 (2010).

[21] M. R. Jarvis, I. D. White, R. W. Godby, and M. C. Payne, Phys. Rev. B **56**, 14972 (1997).

[22] C. A. Rozzi, D. Varsano, A. Marini, E. K. U. Gross, and A. Rubio, Phys. Rev. B **73**, 205119 (2006).

[23] S. Ismail-Beigi, Phys. Rev. B **73**, 233103 (2006).

[24] M. Otani, and O. Sugino, Phys. Rev. B **73**, 115407 (2006).

[25] R. N. Barnett, and U Landman, Phys. Rev. B **48**, 2081-2097 (1993).

[26] D. Marx, J. Hutter, and M. Parrinello, Chem. Phys. Lett. **241**, 457-462 (1995).

[27] G. J. Martyna, and M. E. Tuckerman, J. Chem. Phys. **110**, 2810 (1999).

[28] I. Dabo, B. Kozinsky, N. E. Singh-Miller, and N. Marzari, Phys. Rev. B **77**, 115139 (2008).

[29] A. Y. Lozovoi, and A. Alavi, Phys. Rev. B **68**, 245416 (2003).

[30] J. Neugebauer, and M. Scheffler, Phys. Rev. B **46**, 16067 (1992).

[31] L. Bengtsson, Phys. Rev. B **59**, 12301-12304 (1999).

[32] A. Natan, L. Kronik, and Y. Shapira, Appl. Surf. Sci. **252**, 7608-7613 (2006).

[33] J. R. Chelikowsky, M. M. G. Alemany, T.-L. Chan, and G. M. Dalpian, Rep. Prog. Phys. **74**, 046501 (2011).

[34] PARSEC has a website at `http://parsec.ices.utexas.edu`.

[35] A. Natan, A. Benjamini, D. Naveh, L. Kronik, M. L. Tiago, S. P. Beckman, and J. R. Chelikowsky, Phys. Rev. B **78**, 075109 (2008).

[36] T.-L. Chan, S. B. Zhang, and J. R. Chelikowsky Phys. Rev. B **83**, 245440 (2011).

[37] P. Hohenberg, and W. Kohn, Phys. Rev. **136**, B864 (1964).

[38] W. Kohn, and L. J. Sham, Phys. Rev. **140**, A1133 (1965).

[39] N. Troullier, and J. L. Martins, Phys. Rev. B **43**, 1993 (1991).

[40] L. Kleinman, and D. M. Bylander, Phys. Rev. Lett. **48**, 1425 (1982).

[41] D. M. Ceperley, and B. J. Alder, Phys. Rev. Lett. **45**, 566 (1980).

[42] J. P. Perdew, and A. Zunger, Phys. Rev. B **23**, 5048 (1981).

[43] C. Kittel, Introduction to Solid State Physics, 8th edition, Wiley (2004)

[44] J. E. Lennard-Jones, and M. Dent, Trans. Faraday Soc. 24, 92 (1928).

[45] J. Ihm, A. Zunger, and M. L. Cohen, J. Phys. C **12**, 4409 (1979).

[46] A. Arnold, and C. Holm, Comp. Phys. Comm. **148**, 327-348 (2002).

[47] T.-L. Chan, M. L. Tiago, E. Kaxirus, and J. R. Chelikowsky, Nano Lett. **8** 586-600 (2008).

[48] J. F. Janak, Phys. Rev. B **18**, 7165 (1978).

[49] L. J. Sham, and M. Schluter, Phys. Rev. Lett. **51**, 1888 (1983); L. J. Sham, and M. Schluter, Phys. Rev. B **32**, 3883 (1985).

[50] Chris G. Van de Walle, and A. Janotti, Phys. Status Solidi B **248** 19-27 (2011).

[51] D. J. Griffith, Introduction to Electrodynamics, 4th edition, Addison-Wesley (2012).

[52] T.-L. Chan, A. J. Lee, and J. R. Chelikowsky Comp. Phys. Comm. **185**, 1564-1569 (2014).